

X.L. Li, F. Collin, J.P.Radu & R. Charlier,

MSM Department, University of Liege, Belgium, Member of the ALERT GEOMATERIALS network

**ABSTRACT:** A complete thermo-hydro-mechanical model is presented to tackle the complex coupling problems encountered in clay barriers. A detailed formulation coupling the heat, moisture (liquid water and water vapour) and, air transfer in a deformable unsaturated soil is given. The formulation of the Alonso-Gens's mechanical model for unsaturated soil is also incorporated. The sensitivity to some parameters and their determinations are analysed. Finally, a small scale wetting – heating test on compacted bentonite is performed for validation; the numerical results are compared to the experimental measurements.

## 1.INTRODUCTION

Some nuclear waste disposal concepts are based on storage in deep geological clay layers. The nuclear canisters are surrounded by highly compacted clay, which undergoes a very high suction (up to 100 MPa or more). The present paper deals with the mechanical behaviour of this kind of very hard soils.

The evaluation of the clay barrier efficiency and durability does indeed remain an open question. The partial water saturation of clay implies capillary pressures within the soil pores, which modifies the permeability and the mechanical behaviour with respect to the well known saturated behaviour. Moreover waste is subjected to exothermic reactions (nuclear fission); the confinement barrier is thus subjected to high temperatures (over 70°C or even 100°C).

The design of a clay barrier should take all these phenomena into account. For this purpose, constitutive laws have been developed, coupling the water flow, the heat flow and the soil mechanical properties. They have been implemented in a finite element code which enables to analyse non homogenous transient problems.

The mechanical behaviour of unsaturated soils depends on the stress level and the suction, i.e. the difference between the air and water pore pressures. A first model is established based on classical constitutive laws (e.g. Drucker-Prager's model) and taking into account the suction by means of the Bishop's postulate, which itself extends the

Terzaghi's postulate. A more refined model has been proposed ten years ago by Alonso and Gens; it is based on the CamClay model with the suction level modifying the yield surface, the elastic and hardening parameters.

The water flow in unsaturated media is obeying the same laws as in saturated ones, except that the permeability and storage coefficients depend on the saturation. The problem is then non linear. But high temperature induces the production of water vapour (depending also on the suction level) which flows within the gaseous phase and transports water and heat. This effect appears to be highly significant for the clay material near hot waste. Its modelling is based on Philip and de Vries's contribution.

The developed finite elements possess the following degrees of freedom : displacements of the soil skeleton, temperature, liquid water pressure, and gas (dry air + vapour) pressure. The elements have a monolithical form. All coupling terms of the Newton-Raphson matrix are taken into account, providing a good convergence rate for most treated problems.

A validation of the constitutive laws and finite element code is obtained by comparison with other codes and with some experimental results.

## 2. DIFFUSION MODEL

The design of clay barriers requires the study of the mechanical and the hydraulic behaviours of each component. In this first part, the hydraulic behaviour

of clay will be described and a constitutive flow law will be presented.

In clay barriers, the unsaturated conditions and the thermal solicitations create several couplings effects which will be later commented upon.

Moreover a high temperature under unsaturated conditions induces the production of water vapour. Thus, the medium is composed of three phases (solid, liquid and gas) and three components (water, dry air and solid). The liquid water and the dissolved air form the liquid phase. The gaseous phase is a mixture of dry air and water vapour.

The variables chosen for the description of the flow problem are the liquid water pressure, the gas pressure and the temperature.

The balance equations are written for the mass of the water species (liquid and vapour phases), of the dry air and for the enthalpy of the system.

Motion and state equations will be given for each component of the medium.

## 2.1 Water species

The mass conservation equation is written for the mass of liquid and vapour phases; so the flow of the water species combines the corresponding liquid and vapour flows

The effects of the vapour flow will be significant only if the liquid and vapour flows are of the same order of magnitude. Clay presents a very low permeability: the liquid water motions will be very slow. So the effect of water vapour transport in this type of soil may not be neglected.

### 2.1.1 Mass conservation for the water

The equation includes the variation of the water storage and the divergence of water flows, including the liquid and vapour effects:

$$\frac{\partial S_w}{\partial t} + \text{div}(\underline{V}_w) + \frac{\partial S_v}{\partial t} + \text{div}(\underline{V}_v) = 0 \quad (2.1)$$

with  $S_w = \rho_w \theta_w = \rho_w n S_{r,w}$

$$\underline{V}_w = \rho_w \underline{f}_w$$

$$S_v = \rho_v \theta_v = \rho_v n S_{r,g}$$

$$\text{and } \underline{V}_v = \rho_v \underline{f}_v + \rho_v \underline{f}_g$$

i.e. the vapour flow has two origins: the vapour diffusion in the medium and the gas convection. In these definition formulas,

$\rho_w$  = liquid water density;

$\theta_w$  = volumetric water content;

$n$  = porosity of the medium;

$S_{r,w}$  = saturation degree;

$\underline{f}_w$  = macroscopic velocity of liquid water

= Darcy's velocity;

$\rho_v$  = water vapour density;

$\theta_v$  = volumetric water vapour content;

$S_{r,g} = 1 - S_{r,w}$ ;

$\underline{f}_v$  = macroscopic velocity of the water vapour

= diffusion velocity;

$\underline{f}_g$  = macroscopic velocity of gas;

$t$  = time.

### 2.1.2 Motion of the liquid water

The liquid water velocity is given by the generalised Darcy's law for a multiphase porous medium:

$$\underline{f}_w = - \frac{k_{\text{int}} k_{r,w}}{\mu_w} [\nabla p_w + g \rho_w \nabla y] \quad (2.2)$$

where  $p_w$  = water pressure;

$y$  = vertical, co - ordinate pointing upwards;

$g$  = gravity acceleration;

$\mu_w$  = dynamic viscosity of liquid water;

$k_{\text{int}}$  = intrinsic permeability of the medium;

$k_{r,w}$  = water relative permeability.

In unsaturated conditions, the water permeability varies with respect to the saturation degree.

### 2.1.3 State equation of liquid water

The dynamic viscosity  $\mu_w$  is assumed to depend only on temperature  $T$ . A linear relationship is chosen:

$$\mu_w(T) = \mu_{w0} - \alpha_w^T \mu_{w0} (T - T_0) \quad (2.3)$$

The liquid water density  $\rho_w$  depends on temperature  $T$  and water pressure  $p_w$ . It is given by a linear relationship:

$$\rho_w(T, p_w) = \rho_{w0} \left[ 1 + \frac{p_w - p_{w0}}{\chi_w} - \beta_w^T (T - T_0) \right] \quad (2.4)$$

The saturation degree  $S_{r,w}$  is a function of suction defined as  $s = p_g - p_w$ , where  $p_g$  is the gas pressure. This relationship is based on the retention curve.

The water relative permeability  $k_{r,w}$  relates the decrease of permeability to decrease of saturation  $S_{r,w}$ .

#### 2.1.4 Couplings between the liquid water and other variables

The liquid water properties (i.e. density and viscosity) depend on temperature. This creates a coupling between the liquid water flow and the thermal flow: some convective water flows can thus be created due to the temperature distribution.

Another coupling is due to the permeability which depends on suction: the suction field will influence the water flows.

#### 2.1.5 Diffusion of water vapour

The flow expression for the water vapour is based on Philip and de Vries's model (Philip & de Vries 1957):

$$\underline{f}_v = -[D_{am} \nu_v \tau_v \theta_g / \rho_v] \nabla \rho_v \quad (2.5)$$

where  $\theta_g$  = volumetric gas content;

$D_{am}$  = diffusion coefficient;

$\nu_v$  = 'mass flow' factor;

$\tau_v$  = tortuosity.

This relation is very similar to Fick's law for diffusion and shows that the vapour diffusion is due to a gradient of vapour density.

#### 2.1.6 State equation of water vapour

The diffusion coefficient  $D_{am}$  is suggested as (Krisher & Rohnalter 1940):

$$D_{am} = 5.893 \cdot 10^{-6} \frac{T^{2.3}}{p_g} \quad (2.6)$$

$$p_g = p_a + p_v \quad (2.7)$$

where  $p_a$  = dry air pressure;

$p_v$  = water vapour pressure.

Notice that the diffusion coefficient depends not only on temperature but also on gas pressure.

The mass flow factor  $\nu_v$  is calculated by:

$$\nu_v = \frac{p_g}{p_g - p_v} \quad (2.8)$$

This factor is introduced to allow for the mass flow of vapour arising from the difference in boundary conditions governing the air and vapour components of diffusion systems (Philip & de Vries 1957).

The water vapour density  $\rho_v$  is given by a thermodynamic relationship (Edlefsen & Anderson 1943):

$$\rho_v = \rho_0 h \quad (2.9)$$

where  $\rho_0$  = density of the saturated water vapour;

$h$  = relative humidity.

The relative humidity  $h$  is given by Kelvin-Laplace's law:

$$h = \exp\left(\frac{\psi g}{R_v T}\right) \quad (2.10)$$

where  $\psi = \frac{p_w - p_g}{\rho_w g}$ ;

$R_v$  = gas constant of water vapour.

The relative humidity allows to take into account adsorption phenomena and capillary effect in the soil.

The density of the saturated water vapour is given by a relationship (Mayhew & Rogers 1976) fitted on thermodynamic data:

$$\frac{1}{\rho_0} = 194.4e^{-0.06374(T-273)+0.1634 \cdot 10^{-3}(T-273)^2} \quad (2.11)$$

The water vapour is considered to be perfect gas and the vapour pressure is given by the law for perfect gas:

$$p_v = \rho_v R_v T \quad (2.12)$$

The gradient of the water vapour density can now be developed in order to compute the vapour flow:

$$\nabla \rho_v = \frac{\rho_0 g h}{R_v T} \nabla \psi + \left[ h \beta - \frac{\rho_0 \psi g h}{R_v T^2} \right] \nabla T \quad (2.13)$$

$$\beta = \frac{\partial \rho_0}{\partial T}$$

The gradient of the water vapour density results from two contributions: an isothermal part due to the suction gradient and a thermal part due to the temperature gradient.

A corrective term (Philip & de Vries 1957) in the thermal part is introduced to account for the microscopic effect of heat flow paths shared between sections of solid and fluids paths, this gives rise to microscopic temperature gradients in the fluid filled pores much higher than macroscopic gradients across the sample as a whole.

$$\underline{\nabla}\rho_v = \frac{\rho_0 g h}{R_v T} \underline{\nabla}\psi + \frac{(\nabla T)_a}{\nabla T} \left[ h\beta - \frac{\rho_0 \psi g h}{R_v T^2} \right] \underline{\nabla}T \quad (2.14)$$

The corrective term is written as:

$$\frac{(\nabla T)_a}{\nabla T} = 1/3 \left[ \frac{2}{1+BG} + \frac{1}{1+B(1-2G)} \right]$$

$$B = \frac{(\lambda_a + \lambda_v)}{\lambda_w} - 1$$

if  $0.09 < \theta_w < n$

$$G = 0.3333 - 0.325n(1 - S_{r,w}) \quad (2.15)$$

else

$$G = 0.3333$$

$$+ 11.11 \left[ 0.33 - 0.325 \frac{(n - 0.09)}{n} \right] \theta_w$$

$$\lambda_v = D_{am} \nu_v h L \beta$$

where  $L$  is the latent heat of vaporisation.

### 2.1.7 Couplings between the water vapour and other variables

As shown above, the vapour properties and flows depend essentially on the temperature and gas pressure fields.

This model can reproduce the transport of water vapour from high temperature points (where vapour is produced) to lower temperature points (where vapour condenses).

## 2.2 Dry air species

The choice is made to write the balance equation on the term of the dry air mass. Dry air is a part of a gas mixture: the gas phase is composed by dry air and water vapour. But there is also air dissolved in the water which has to be taken into account.

The dry air pressure is not a basic variable: this pressure will be computed up to the gas and the vapour pressure.

Dalton's law is assumed: the pressure of the gas mixture is equal to the sum of the partial pressures which each gas would exert if it filled alone all the volume considered.

### 2.2.1 Mass conservation for the dry air

The equation of mass conservation includes the contributions of the dry air phase and the air dissolved in water:

$$\frac{\partial S_a}{\partial t} + \text{div}(\underline{V}_a) + \frac{\partial S_{a,dissolved}}{\partial t} + \text{div}(\underline{V}_{a,dissolved}) = 0 \quad (2.16)$$

$$\text{with } S_a = \rho_a \theta_g = \rho_a n S_{r,g}$$

$$\underline{V}_a = \rho_a \underline{f}_g$$

$$S_{a,dissolved} = H \rho_a \theta_w = H \rho_a n S_{r,w}$$

$$\underline{V}_{a,dissolved} = H \rho_a \underline{f}_w$$

where  $\rho_a$  = dry air density.

The Henry's coefficient  $H$  allows to determine amount of air dissolved in the liquid water. The dissolved air mass is supposed to be sufficiently low so that the water properties not be influenced.

The dry air flow is due to the flow of the gas mixture which has to be defined.

### 2.2.2 Motion of gas

The gas velocity is given by generalised Darcy's law for multiphase medium:

$$\underline{f}_g = - \frac{k_{mt} k_{r,g}}{\mu_g} \left[ \underline{\nabla}p_g + g \rho_g \underline{\nabla}y \right] \quad (2.17)$$

where  $\mu_g$  = dynamic viscosity of the gas;

$k_{r,g}$  = relative permeability of the gas;

$\rho_g$  = gas density.

The gas permeability is adapted to reproduce its variation in non-saturated conditions.

### 2.2.3 State equation of the gas

Being a mixture of dry air and vapour, the gas properties will be defined through the properties of the components.

The dynamic viscosity  $\mu_g$  is obtained by means of a mixture law (Wilke 1950):

$$\mu_g = \frac{\mu_a}{1 + \frac{(x_v/x_a) \left[ 1 + (\mu_a/\mu_v)^{0.5} (M_v/M_a)^{0.25} \right]^2}{(4/\sqrt{2}) \left[ 1 + (M_a/M_v) \right]^{0.5}}} + \frac{\mu_v}{1 + \frac{(x_a/x_v) \left[ 1 + (\mu_v/\mu_a)^{0.5} (M_a/M_v)^{0.25} \right]^2}{(4/\sqrt{2}) \left[ 1 + (M_v/M_a) \right]^{0.5}}} \quad (2.18)$$

where  $x_a = p_a / p_g =$  dry air mole fraction;

$x_v = p_v / p_g =$  vapour mole fraction;

$M_v =$  vapour molecular weight;

$M_a =$  dry air molecular weight.

The dynamic viscosity of dry air  $\mu_a$  is given by a linear relationship:

$$\mu_a(T) = \mu_{a0} - \alpha_a^T \mu_{a0} (T - T_0) \quad (2.19)$$

The dynamic viscosity of vapour  $\mu_v$  is given by (Speyerer 1923):

$$\mu_v(T) = 125.4 \cdot 10^{-7} + 3.711 \cdot 10^{-8} (T - 373) \quad (2.20)$$

The gas density  $\rho_g$  is not directly known but the following relationship is assumed :

$$\rho_g = \rho_a + \rho_v \quad (2.21)$$

Dry air is considered as a perfect gas; it thus respects the equation:

$$\rho_a(T, p_a) = \rho_{a,0} \frac{p_a}{p_{a,0}} \frac{T_0}{T} \quad (2.22)$$

In this expression, the dry air pressure is not known directly but is equal to the difference between total gas pressure and vapour pressure.

The gas saturation degree  $S_{r,g}$  is defined by  $S_{r,g} = 1 - S_{r,w}$  and therefore a new relationship does not need to be introduced.

The gas relative permeability  $k_{r,g}$  relates the increase of gas permeability to the decrease of water saturation degree  $S_{r,w}$ .

## 2.2.4 Couplings

The couplings have the same origin as in the liquid water case.

## 2.3 Heat diffusion

### 2.3.1 Conservation of the heat

$$\frac{\partial S_T}{\partial t} + \text{div}(\underline{V}_T) - Q = 0 \quad (2.23)$$

where  $S_T = \phi =$  enthalpy;

$\underline{V}_T = \underline{q} =$  heat flow;

$Q =$  volume heat source.

### 2.3.2 Quantity of heat storage: Enthalpy

The enthalpy of the system is the sum of the enthalpies of the medium components:

$$\phi = \phi_w + \phi_a + \phi_s + \phi_v + \phi_{Latent} \quad (2.24)$$

with  $\phi_w = nS_{r,w} \rho_w c_{p,w} (T - T_0)$ ;

$\phi_a = nS_{r,g} \rho_a c_{p,a} (T - T_0)$ ;

$\phi_s = (1 - n) \rho_s c_{p,s} (T - T_0)$ ;

$\phi_v = nS_{r,g} \rho_v c_{p,v} (T - T_0)$ ;

$\phi_{Latent} = nS_{r,g} \rho_v L$ ;

$c_{p,\alpha} =$  specific heat of the component  $\alpha$ .

(2.25)

The last enthalpy term corresponds to the heat stored during water vaporisation.

### 2.3.3 Heat transport

Three heat transport terms are taken into account: they represent the conductive, convective and vaporisation effects.

$$\underline{q} = \underline{q}_{conduction} + \underline{q}_{convection} + \underline{q}_{latent} \quad (2.26)$$

$$\underline{q}_{cond} = -\Gamma \nabla T$$

$$\underline{q}_{conv} = \phi_w \underline{f}_{w,eff} + \phi_a \underline{f}_{g,eff} + \phi_v \underline{f}_{g,eff}$$

$$+ c_{pv} \rho_v \underline{f}_v (T - T_0)$$

$$\underline{q}_{latent} = (\rho_v \underline{f}_v + \rho_v \underline{f}_g) L \quad (2.27)$$

$$\text{with } \underline{f}_{w,eff} = \frac{\underline{f}_w}{nS_{r,w}} \text{ and } \underline{f}_{g,eff} = \frac{\underline{f}_g}{nS_{r,g}};$$

$\Gamma =$  conductivity of the medium.

The solid convection is also explicitly modelled by some authors. Our model is taking the large strains and large rotation of the sample into account, thanks to a updated Lagrangian formulation. Therefore the equilibrium and balance equation, as well as the water, air, and heat flow, are expressed in

the current configuration. This is implicitly takes into account the solid convection effect.

### 2.3.4. Couplings

The main coupling results from the convection: a certain amount of heat is transported by the water, vapour and air flows. Consequently the temperature field can be modified.

## 3 MECHANICAL BEHAVIOUR MODELLING

In a clay barrier, the saturation and the suction can vary considerably. Research experiments have shown that the suction has a strong influence on the mechanical properties: the hardness and the shear strength of the soil increase with suction; the swelling or collapse can be induced; some irreversible deformations can even take place...

The mechanical behaviour modelling should be able to take this suction effect into account when the soil undergoes desaturation processes.

### 3.1 Stress state variables

The choice of stress state variables to describe the stress-strain relation is still an open question. Many researchers (Bishop & Blight 1963) have attempted to incorporate the suction  $s$  explicitly into an *effective stress* expression. For example, Bishop's postulate:

$$\sigma'_{ij} = \sigma_{ij} - p_g \delta_{ij} + \chi(p_g - p_w) \delta_{ij} \quad (3.1)$$

where  $\sigma'_{ij}$  is the effective stress tensor,  $\sigma_{ij}$  is the total stress tensor,  $\chi$  represents the Bishop's coefficient which is a function of the saturation  $S_{r,w}$ ,  $\delta_{ij}$  refers to the Kronecker's tensor.

This concept presents some advantages: it is easy to implement into a finite element code (Schrefler et al. 1996, Charlier et al. 1997); it provides qualitatively good predictions for problems involving mainly shear stresses...

But its application to modelling of the mechanical behaviour of unsaturated soils is limited mainly because of the following reasons:

1. Generally, the volumetric behaviour cannot be properly modelled with this postulate. In particular, it is unable to model the collapse behaviour, which is a typical phenomenon of unsaturated soils during the wetting phase under certain external charges.

2. The Bishop's coefficient  $\chi$  is a very complicate function. Experimental investigations (Jennings &

Burland 1962) have shown that it may depend on the saturation  $S_{r,w}$  but there is non-unique relation  $\chi - S_{r,w}$  for a given soil sample with different void ratios.

3. The value of the  $\chi$  is stress path dependant.

4. The experimental determination of  $\chi$  is very difficult.

However, a simplified Bishop's postulate with  $\chi = S_{r,w}$  has been implemented in the LAGAMINE code in order to model problems where the shear strain is dominant; it can be incorporated in any classical model (e.g. Drucker-Prager's model).

All these considerations lead to using the *independent stresses state variables* to model the mechanical behaviour of unsaturated soils. That is:

$$\begin{aligned} \text{the net stresses tensor : } \sigma_{ij}^* &= \sigma_{ij} - p_g \delta_{ij} \\ \text{the suction : } s &= p_g - p_w \end{aligned} \quad (3.2)$$

It is proved to be suitable for the modelling of the mechanical behaviour of unsaturated soils from the theoretical as well as the experimental points of view (Fredlund & Morgenstern 1977).

### 3.2 Alonso-Gens's mechanical model

The model proposed by Alonso et al (Alonso et al. 1990) is based on the well-known CamClay model. It is written within the framework of the *independent stresses state variables* defined here above. In our finite element code LAGAMINE, the plastic yield surfaces are written in a three-dimensional stress space:  $I_\sigma^* - II_\sigma^* - s$  where  $I_\sigma^*$  is the first net stress invariant and  $II_\sigma^*$  refers to the second net deviatoric stress invariant.

#### 3.2.1 The yield surfaces

The yield surface in the  $I_\sigma^* - II_\sigma^*$  space, named  $F_I$ , is written for a given value of suction as:

$$F_I = \left( I_\sigma^{*2} + (I_0 - P_s) I_\sigma^* - I_0 P_s \right) \bar{r}^2 + II_\sigma^{*2} \quad (3.3)$$

where  $\bar{r}$  is defined as a *reduced radius* which represents the failure states and is given by:

$$\bar{r} = \frac{II_\sigma^*}{I_\sigma^*} \quad (3.4)$$

It can depend or not on the Lode's angle  $\alpha$ , according to (Fig. 3.1):

$$\bar{r} = \begin{cases} C^{te} & \text{Von-Mises} \\ a(1+b*\sin 3\alpha)^n & \text{Van-Eekelen} \end{cases} \quad (3.5)$$

$a$ ,  $b$ ,  $n$  are constants which are linked to the internal friction angles in compression and extension; they may vary with the suction.

$P_s$  represents the soil strength in extension, given by:

$$P_s = 3c / \text{tg} \phi_c \quad (3.6)$$

where  $c$  is the cohesion and  $\phi_c$  refers to the internal friction angle in compression. Both  $c$  and  $\phi_c$  may vary with suction; functions  $c(s)$  and  $\phi_c(s)$  based on experimental results can be introduced into the code.

$I_0$  represents the pre-consolidation of soil and varies with the suction (Fig. 3.2):

$$I_0 = p_c \left( \frac{I_0^*}{p_c} \right)^{\frac{\lambda(0)-\kappa}{\lambda(s)-\kappa}} \quad (3.7)$$

where  $I_0^*$  represents the pre-consolidation pressure of soil in saturated condition;  $p_c$  is a reference pressure;  $\lambda(s)$  refers to the plastic slope of the compressibility curve against the net mean stress, it varies with the suction according to:

$$\lambda(s) = \lambda(0) [(1-r) \exp(-\beta s) + r] \quad (3.8)$$

here  $\lambda(0)$  is the plastic slope for the saturated condition.  $\kappa$ , the elastic slope of the compressibility curve against the net mean stress, may also be function of the suction.  $r$  and  $\beta$  are parameters describing the changes in soil stiffness with suction.

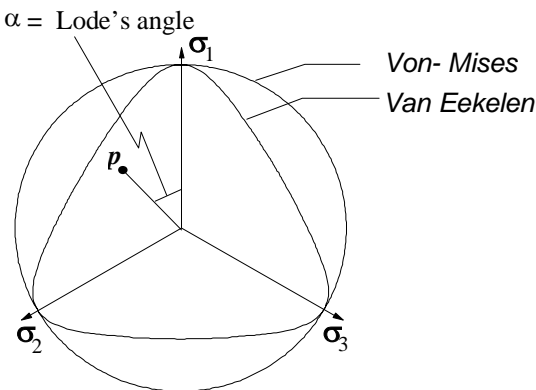


Fig. 3.1 Yield surface : Lode's angle dependence

The yield surface ( $SI$ ) in the  $I_\sigma^* - s$  plane, named  $F_2$ , is given by (Fig. 3.2):

$$F_2 = s - s_0 \quad (3.9)$$

where  $s_0$  is a yield value which represents the maximum suction submitted by the soil.

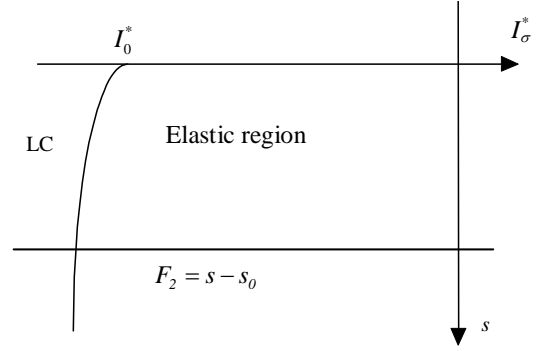


Figure 3.2. Yield surface in the  $I_\sigma^* - s$  plane

The trace of the preconsolidation pressure in the  $I_\sigma^* - s$  plane (equation 3.7) defines another part of the yield surface called LC (Loading Collapse) used for modelling the collapse behaviour under wetting.

### 3.2.2 Responses of the model

The elastic and plastic strains due to the stress (mechanical solicitations) are calculated by:

$$\dot{\epsilon}_{kl-m}^e = C_{ijkl}^{e-1} \dot{\sigma}_{ij}^e \quad (\text{elastic deformations}) \quad (3.10)$$

$$\dot{\epsilon}_{ij-m}^p = \dot{\lambda} \frac{\partial Q}{\partial \sigma_{ij}^*} \quad (\text{plastic deformations}) \quad (3.11)$$

where  $C_{ijkl}^e$  is the Hooke's tensor,  $\dot{\sigma}_{ij}^e$  is the elastic net stress tensor,  $Q$  is the symbol for the plastic potential surface, and  $\dot{\lambda}$  is obtained by the consistency condition.

A non-linear elasticity can be considered by means of:

$$K = \frac{1+e}{3\kappa} I_\sigma^* \quad (3.12)$$

$$G = \frac{3(1-2\nu)}{2(1+\nu)} K$$

where  $K$  is the soil bulk modulus,  $G$  its shear modulus,  $\nu$  its Poisson's coefficient and  $e$  its void ratio.

A non-associated flow rule in the  $I_\sigma^* - II_\sigma^*$  plane can be introduced into the model via the following equations:

$$\frac{\partial Q}{\partial II_\sigma^*} = \eta \frac{\partial F}{\partial II_\sigma^*} \quad (3.13)$$

where  $\eta$  is a parameter related to the  $\bar{r}$ ,  $\kappa$ , and  $\lambda(s)$ .

The deformations induced by the suction change (hydraulic path) are :

$$\dot{\epsilon}_{kl-s}^e = h^e \dot{s} \delta_{kl} \quad (\text{elastic deformations}) \quad (3.14)$$

$$\dot{\epsilon}_{kl-s}^p = h^p \dot{s} \delta_{kl} \quad (\text{plastic deformations}) \quad (3.15)$$

$$\text{with } h^e = \frac{\kappa_s}{3(I+e)(s+P_{at})} \quad (3.16)$$

$$h^p = \frac{\lambda_s - \kappa_s}{3(I+e)(s+P_{at})} \quad (3.17)$$

where  $\lambda_s$  and  $\kappa_s$  are stiffness parameters for changes in suction and  $P_{at}$  is the atmospheric pressure. It should be noted that  $\lambda_s$  and  $\kappa_s$  can vary with the stress level.

The plastic deformation in compression due to the suction takes place when the suction is larger than  $s_0$ .

The elastic thermal dilatation is introduced in the model by:

$$\dot{\epsilon}_{kl-T}^e = \xi \dot{T} \delta_{kl} \quad (3.18)$$

where  $\xi$  is the dilatation coefficient.

The evolution of yield surfaces is controlled by the total plastic volumetric strain  $\epsilon_v^p$  developing in the soil via two state variables  $I_0^*$  and  $s_0$ :

$$dI_0^* = \frac{(I+e)I_0^*}{\lambda(\theta) - \kappa} d\epsilon_v^p \quad (3.19)$$

$$ds_0 = \frac{(I+e)(s_0 + P_{at})}{\lambda_s - \kappa_s} d\epsilon_v^p \quad (3.20)$$

After appropriate manipulations, the general constitutive relationship in reverse form can be written as:

$$\dot{\sigma}_{ij} = D_{ijkl} \dot{\epsilon}_{kl} - V_{ij} \dot{s} \quad (3.21)$$

where  $D_{ijkl}$  is the classical elasto-plastic tensor and  $V_{ij}$  is a tensor related to the suction.

For the integration of the constitutive relation, we have used the so-called  $\theta$  point method. To obtain more accurate results, the integration time step  $\Delta t$  is divided into  $N$  sub-steps  $dt$ . The sub-steps size can be automatically adjusted in function of the strain increment  $\|\Delta \epsilon\|$  or chosen by the user. For each sub-

time step  $dt$ , the integration of equation (3.21) can be expressed as:

$$\begin{aligned} \sigma_{ij}(I + \theta dt) &= \sigma_{ij}(I) + \dot{\sigma}_{ij}(I) * \theta dt \\ \sigma_{ij}(I + 1) &= \sigma_{ij}(I) + \dot{\sigma}_{ij}(I + \theta dt) * dt \end{aligned} \quad (3.22)$$

where  $I$  denotes the sub-time step number;  $\theta$  is a numerical parameter that takes the value between 0 and 1 (usually  $\theta > 0.5$  for reasons of numerical stability).

The hardening variables can be also integrated in the same way.

This version of the model can simulate the swelling and collapse behaviours but has some limitations for highly expansive materials: the plastic swelling deformation cannot be taken into account.

### 3.2.3 Sensitivity of the soil parameters

The parameters requested by the model and their determination means are outlined in table 3.1.

Three series of suction controlled tests are required to determine the major parameters. The first one includes oedometer tests with wetting-drying cycles under different but constant vertical pressure. The second series consists of oedometer tests following several loading-unloading cycles under different but constant suctions. The third one should be a series of suctions controlled triaxial tests.

In practice, the determination of the parameters is not always evident. For example, the experimental results are not always easily interpreted; repeated tests do not always reproduce the same results. This throws doubt on the experimental results...

We should note that the yield surface LC governed by equation (3.7) is very sensitive and its convexity is not always guaranteed. Two difficulties are often met during calibration. Firstly we should avoid  $\lambda(s) < \kappa$  in any cases. Secondly, the convexity of the LC is linked with the value of  $p_c$ , this latter is not easily determined directly from experimental results, we have to determine it by a calibration procedure. On the other hand, the LC calibration has an important influence on the model responses. We will show an example of validation tests to illustrate the difficulties during LC calibration.

In the case of non-linear elasticity, the shear module  $G$  depends on the Poisson's ratio  $\nu$  and the stress level. From equation (3.12), we get :

$$G = \frac{3(1-2\nu)(I+e)}{2(1+\nu)} \frac{I_0^*}{3\kappa} = \zeta \frac{(I+e)}{\kappa} I_0^* \quad (3.23)$$

On figure 3.3, we have plotted the proportional coefficient  $\zeta$  in function of  $\nu$ .

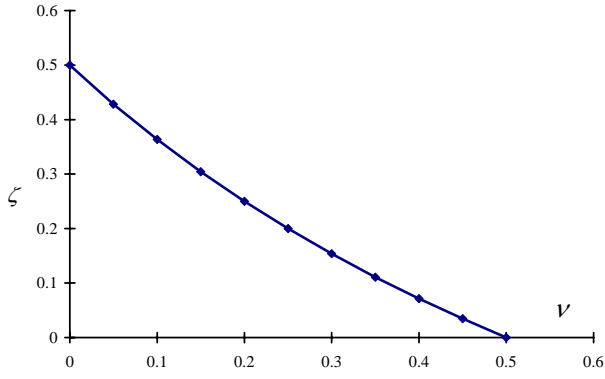


Fig. 3.3 Influence of  $\nu$  on the shear module of soil

We note that, for a given value of stress generated in the soil  $I_{\sigma}^*$ , the shear module  $G$  can decrease more than two times when  $\nu$  changes from 0.3 to 0.4. However, the shear modulus  $G$  plays a most important role for generating the deviatoric stress which in turn control the hardening or softening aspects of the model responses.

Table 3.1. Parameters of the model

Parameters	Determination means
$e_0$	Measured
$\lambda(0)$	Oedometer loading-unloading test in saturated state
$I_0^*$	Id.
$\lambda_s$	Oedometer or isotropic wetting-drying tests under different external charges.
$\kappa_s$	Id.
$r$	Series of suction controlled oedometer tests
$\beta$	Id.
$p_c$	Id. The measurements of $I_0$ at different level of suction are required to calibrate $p_c$
$\kappa$	Id. the function $\kappa(s)$ may be observed
$C(s)$	Series of suction controlled triaxial tests
$\varphi_c(s)$	Id.

#### 4. VALIDATION TESTS

Within the frame of an European Community research project entitled *Calculation and testing of behaviour of unsaturated clay (Catsius clay)*, a small scale wetting-heating test has been performed on highly compacted bentonite. The objective of the test was to investigate both temperature and artificial

hydration effects on the deformation and moisture transfer in the soil.

The test is performed inside a thermohydraulic cell schematised on figure 4.1. The sample is heated by means of the central heater and hydrated through the ports which are connected to the porous plate. During the test, the temperature at different points of soil are monitored by means of the thermocouples, the volume of water flow is also measured. In the mean time, the swelling pressure generated in the sample is measured through pressure transducers. The outer cell surface is in contact with the ambient air.

The experience is carried out by applying a controlled thermal power to the heater and a constant water pressure to the lower porous plate during the experience (2401.6 hours).

A finite element simulation has been performed within the same research project.

The finite element developed for the simulation is a 2D axisymmetric finite element with five coupled degrees of the freedom: soil skeleton displacements, liquid water pressure, gas pressure (sum of the dry air and water vapour pressures), and temperature. The element has a monolithic form, all coupling terms are included in the Newton-Raphson's stiffness matrix, allowing a good convergence rate for most treated problems.

The finite element mesh includes 102 elements representing the bentonite sample, 70 for the steel case, and 7 for the porous plate. In addition, to model the convection transfer between the steel case and the ambient atmosphere, 39 two dimensional frontier thermal elements are also incorporated into the mesh.

The heater action is realised by imposing the temperature on the nodes of the sample in contact with the heater. The hydrated procedure is modelled by increasing the water pressure on the nodes of porous plate.

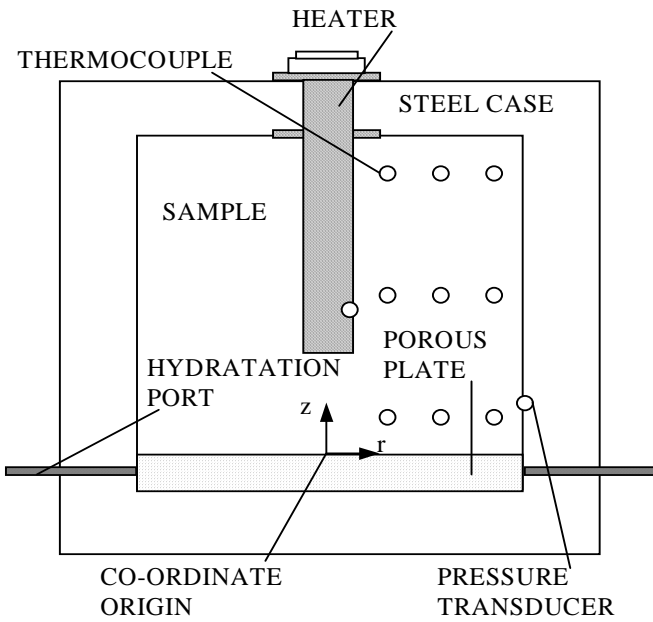


Fig. 4.1 Configuration of the thermohydraulic cell

The steel case is supposed to be impermeable to the water flow. Both steel case and porous plate deformations are neglected. Initially the system is at ambient temperature (293 °K). The gas pressure remains fixed to the atmospheric pressure (100 kPa). The initial soil saturation is 49% which gives an initial suction  $s = 78.6$  MPa according to the water retention curve.

#### 4.1 Hydraulic and thermal properties

The resulting experimental points of the retention curve are not easily interpreted because they do not define one single curve. Anyway a mean numerical curve is chosen in order to approximate the measured data:

$$S_{r,w} = S_{r,res} + CSW3 \frac{(S_{r,field} - S_{r,res})}{CSW3 + (CSW1.s)^{CSW2}} \quad (4.1)$$

where  $S_{r,field}$  is the maximum saturation and  $S_{r,res}$  is the residual saturation for a very high value of suction.

The water relative permeability is determined by:

$$k_{r,w} = \frac{(S_{r,w} - S_{r,res})^{CKW}}{(S_{r,field} - S_{r,res})^{CKW}} \quad \text{if } S_{r,w} \geq S_{r,res} \quad (4.2)$$

$$k_{r,w} = k_{r,w,min} \quad \text{if } S_{r,w} < S_{r,res}$$

The gas relative permeability is modelled by:

$$k_{r,g} = (1 - S_e)^{CKA1} (1 - S_e^{CKA2}) \quad (4.3)$$

$$\text{with } S_e = \frac{S_{r,w} - S_{r,res}}{1 - S_{r,res}}$$

The water retention curve and the permeability are found to have an important influence on the water intake volume and the final saturation degree.

The soil conductivity is a function of the saturation degree, and is given by a linear relationship based on experimental data:

$$\Gamma = CLT1 S_{r,w} + CLT2 \quad (4.4)$$

Steel conducts heat: at the outer boundary, the convection coefficient between ambient air and steel case is equal to  $8 \text{ W/m}^2$ .

The values of the hydraulic and thermal properties are summarized in the table 4.1

Table 4.1 : Hydraulic and thermal properties

$n$	0.4	$c_{p,soil}$	$879 \text{ J kg}^{-1} \text{ K}^{-1}$
$\tau$	0.1	$S_{r,field}$	1.0
$T_0$	293 °K	$S_{r,res}$	0.1
$p_{w,0}$	100 kPa	$CSW1$	$3.5 \cdot 10^{-6}$
$p_{g,0}$	100 kPa	$CSW2$	0.9
$\mu_{w,0}$	$10^{-2} \text{ Pa s K}^{-1}$	$CSW3$	120
$\rho_w$	$1000 \text{ kg m}^{-3}$	$k_{int}$	$4.7 \cdot 10^{-21} \text{ m}^2$
$\chi_w$	$0.333 \cdot 10^{-9} \text{ Pa}^{-1}$	$k_{r,w,min}$	0.01
$\beta_w^T$	$0.38 \cdot 10^{-3} \text{ K}^{-1}$	$CKW$	3
$\lambda_w$	$0.623 \text{ W m}^{-1} \text{ K}^{-1}$	$CKA1$	2
$c_{p,w}$	$4180 \text{ J kg}^{-1} \text{ K}^{-1}$	$CKA2$	0.1667
$\mu_{a,0}$	$-0.25 \cdot 10^{-2} \text{ Pa s K}^{-1}$	$CLT1$	1.0553
$\rho_a$	$1.205 \text{ kg m}^{-3}$	$CLT2$	0.3573
$\lambda_a$	$0.25 \cdot 10^{-1} \text{ W m}^{-1} \text{ K}^{-1}$	$\lambda_{steel}$	$46.50 \text{ Wm}^{-1} \text{ K}^{-1}$
$c_{p,a}$	$1000 \text{ J kg}^{-1} \text{ K}^{-1}$	$c_{p,steel}$	$4610 \text{ J kg}^{-1} \text{ K}^{-1}$
$\xi_{soil}$	$0.2312 \cdot 10^{-3} \text{ K}^{-1}$		

#### 4.2 Parameters related to the mechanical model

Two series of suction controlled oedometer tests have been performed. The first one consists of wetting-drying cycles under different constant vertical pressures. Tests of the second series are performed following several loading-unloading cycles under different constant suctions.

In spite of difficulties to interpret the experimental results, these two series of tests provide some fundamental parameters for Alonso-Gens's model (Fig.4.2, 4.3, 4.4) which show immediately that:

1.  $\kappa$  effectively depends on the suction imposed in the sample (Fig.4.2);

2.  $\kappa_s$  varies with the imposed vertical stress. It implies that  $\kappa_s$  may be dependent on the stresses generated in the sample (Fig.4.3);

3.  $\lambda$  decreases with the suction (Fig.4.4).

For what concerns the *LC* curve, it is controlled by equation 3.7 and equation 3.8. These two equations are numerically interrelated. In practice, many difficulties are encountered to find one set of parameters to satisfy these two equations at the same time. For example, if the calibration of parameters  $r$ ,  $\beta$  and  $p_c$  is based on equation (3.7), a relative good correlation of the *LC* curve with experimental results is obtained (fig.4.5); but the calculated plastic stiffness parameter for high value of suction  $\lambda(s)$  seems to be too high with respect to the experimental results (fig.4.4). However if parameters  $r$  and  $\beta$  are calibrated with equation (3.8), the numerical values of  $\lambda(s)$  correlate better with the experimental ones (fig.4.4); but the *LC* curve is far away from the measured values in this case. In fact, the problem is that the *LC* curve is very sensitive to  $p_c$  value. In other words, the  $p_c$  value is not guaranteed since it is not easily determined from available experimental results.

The parameters used for the validation test are listed in table 4.2.

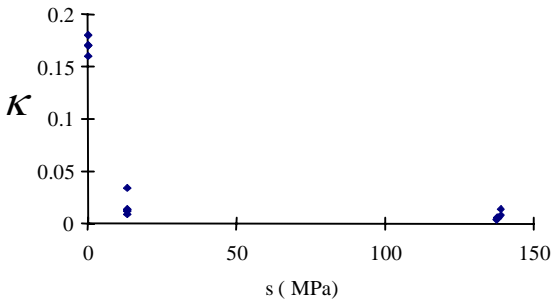


Fig.4.2 Elastic stiffness parameter for changes in net mean stresses in function of the suction

The parameters related to the shear strength are not available since there are no suction controlled triaxial tests are performed. By the way, the suction yield parameter  $s_0$  is obtained by the water retention curve.

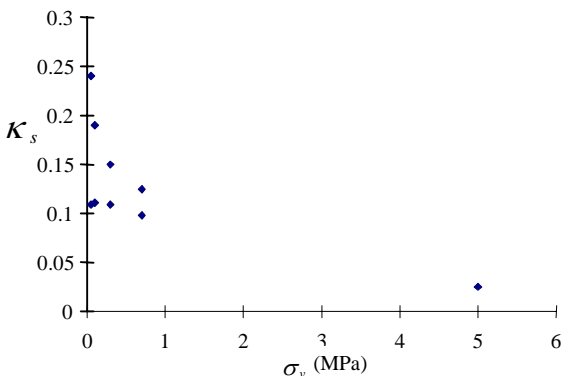


Fig. 4.3 Elastic stiffness parameter for changes in suction in function of the vertical charges

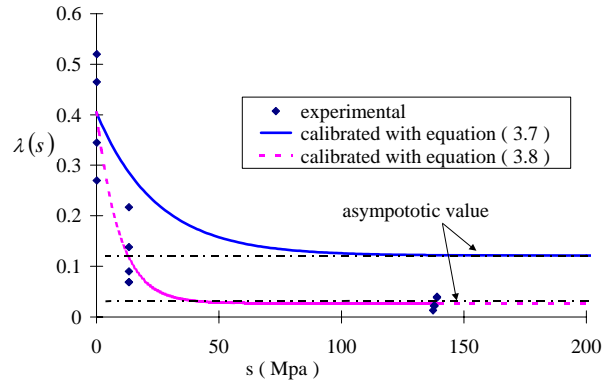


Fig. 4.4 Plastic stiffness parameters for changes in net mean stresses in function of the suction

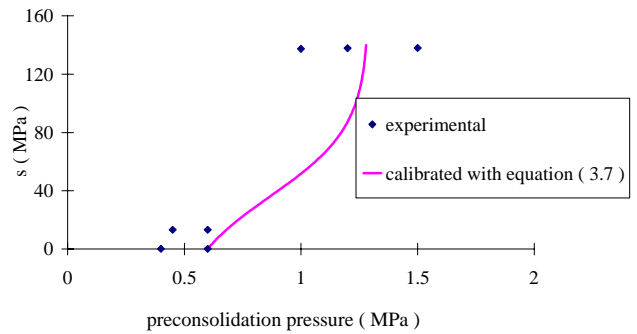


Fig. 4.5 Calibration of parameters related to the *LC* curve based on the equation (3.7)

Table 4.2 Some fundamental parameters used for the simulation

$\lambda(0)$	0.4041	$\lambda_s$	0.25
$\kappa$	0.015	$p_c$	0.45
$p_0^*$	0.6 MPa	$r$	0.3
$\kappa_s$	0.11	$\beta$	$0.041 \text{ MPa}^{-1}$

### 4.3 Comparisons between simulation and experimental results

Figure 4.6 shows the water intake evolution with time. A very good result is obtained: the experimental and numerical curves are almost the same. It should be noticed that the numerical result depends not only on the permeability curve but also on the retention curve and the temperature field.

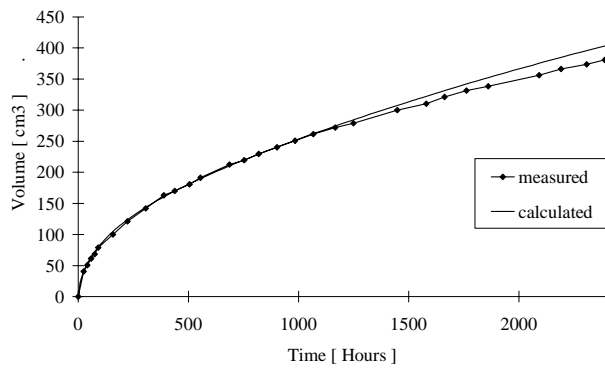


Fig. 4.6 Water intake evolution

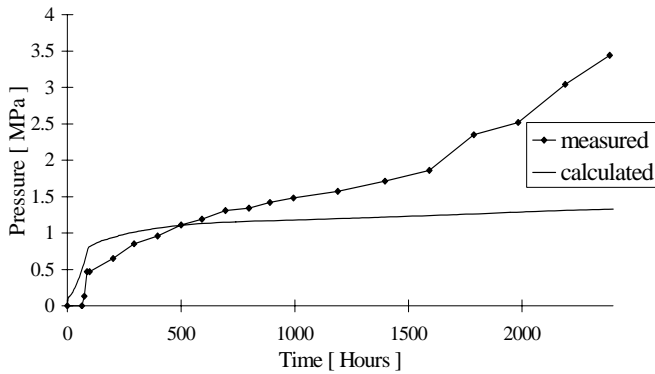


Fig. 4.7 Swelling pressure evolution

The swelling pressure at the point with coordinates  $r=7.5$  cm and  $z=1.25$  cm is recorded during the experiment. The comparison between experimental and numerical results is shown on figure 4.7. The agreement is good at the beginning, but deteriorates towards the end. As discussed before, the parameters related to the mechanical model are very difficult to determine. A better simulation result might be obtained if all variations of the parameters were taken into account, like the fact that  $\kappa_s$  varies with the net stress,  $\kappa$  depends on the suction, etc.

Figure 4.8 gives the calculated isotherm lines after 2380.6 hours. The experimental measurements at some points at this same time are also indicated on the figure. The calculated temperatures are slightly higher than the experimental ones.

The calculated level curves of the water content at the end of experiment are given on the figure 4.9. The measurements at some points are also presented on the same figure. The numerical results seem to be slightly lower than the experimental ones at the analysed points. But the result near the heater is relatively good: the numerical water content is close to the experimental one. Here the generation of water vapour near the heater is a crucial phenomenon to be taken in account. The vapour flow depends deeply on the temperature.

All results appear to be very sensitive to the retention curve, the relative and intrinsic permeability.

A last remark could be made that the soil mechanics has a small influence on the water flow. On the contrary, the water flow has a strong influence on the mechanical behaviour.

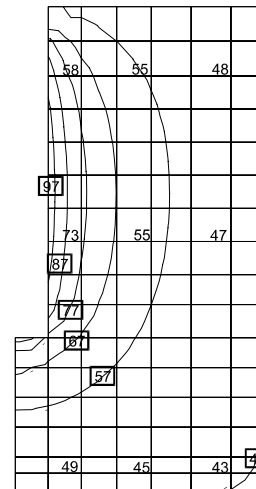


Fig.4.8 Temperature field at the end of the experiment

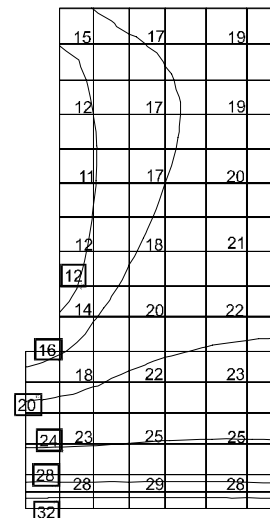


Fig.4.9 Water content at the end of the experiment

## 5. CONCLUSION

A complete theory of a thermo-hydro-mechanical coupling model for unsaturated soils is provided in this paper. A validation test is performed to show the capabilities of the model to simulate the relevant phenomenon in a nuclear energy storage. The comparison between simulation results and experimental ones is discussed. Some sensitivities of the mechanical parameters are also mentioned.

## ACKNOWLEDGEMENTS

The authors thank the Europe Community for the support through the research project *Catsius clay* project. The support from FNRS is also greatly acknowledged.

## REFERENCES

- Alonso, E.E. & Gens, A. & Josa, A.A. 1990. A constitutive model for partly saturated soil. *Géotechnique*. 40, n°3: 405-430.
- Bishop, A.W. & Blight, G.E. 1963. Some aspects of effective stress in saturated and unsaturated soils. *Géotechnique*. n°3: 177-197.
- Charlier, R. & Radu, J.P. 1997. Hydro-mechanical coupling and strain localisation. *Proc. NAFEMS World Congress*.
- Edlefsen, N. E. & Anderson, A.B.C. 1943. Thermodynamics of soils moisture. *Hilgardia* 15, No. 2, 31-298.
- Fredlund, D.G. & Morgenstern, N.R. 1977. Stress state variables for unsaturated soils. *J. Geotech. Eng. Div. A.S.C.E.* 103 GT5. 447-466.
- Jennings, J.E.B. & Burland, J.B. 1962. Limitations to the use of effective stresses in partly saturated soils. *Géotechnique*.12, n°2: 125-144.
- Krisher, O. & Rohnalter, H. 1940. Wärmeleitung und dampfdiffusion in feuchten gutern. *Verein. Deut. Ing.-Forschungsheft*,402.
- Mayhew, Y.R. & Rogers, G.F.C. 1976. Thermodynamic and transport properties of fluids. 2<sup>nd</sup> edn., *Oxford: Blackwell*.
- Philip, J.R. & de Vries, D.A. 1957. Moisture movement in porous materials under temperature gradients. *Trans. Am. Geophys. Un.* 38, 222-232.
- Schrefler, B.A. & Simoni, L. & Li, X.K. & Zienkeiwicz, O.C. 1990. Mechanics of partially saturated porous media. In Numerical methods and constitutive modelling in geomechanics. C.S. Desai and G. Gioda, ed. *CISM Courses and Lectures*, N° 311, *Springer Verlag*, 169-209.
- Speyerer, H. 1923. *Zeit. für techn. Physik.* 4(11), pp. 430.
- Wilke, C.R. 1950. A viscosity equation for gas mixtures. *Jnl. Chem. Physics*, 18(4), 517-519